JAAS

ROYAL SOCIETY OF CHEMISTRY

PAPER

View Article Online
View Journal | View Issue

Cite this: *J. Anal. At. Spectrom.*, 2023, **38**, 1253

Investigation of matrix effects in nitrogen microwave inductively coupled atmospheric-pressure plasma mass spectrometry (MICAP-MS) for trace element analysis in steels†

Alexander Winckelmann, [ab] Janina Roik,[a] Sebastian Recknagel,[a] Carlos Abad *[a] and Zengchao You*[a]

We investigated the performance of nitrogen microwave inductively coupled atmospheric-pressure plasma mass spectrometry (MICAP-MS) under matrix effects and its applicability to trace element analysis in steels. Influences of different gas flows and ion optics on the matrix tolerance are studied, indicating that nebulizer gas flow has the most significant impact. Optimization of ion optics improves matrix tolerance for light elements due to the reduction of the inelastic collisional scattering effect. With optimized operating conditions, MICAP-MS achieves an internal standard intensity recovery of over 90% at an Fe concentration of 500 mg L^{-1}. Even at an Fe concentration of 1 g L^{-1}, the recovery remains above 80%. Three certified reference materials – non-alloy, low-alloy and high-alloy steel – were analyzed using MICAP-MS. The determined mass concentrations of the trace and minor components show metrological compatibility to the reference values. No significant differences are observed between the results obtained with aqueous and matrix-matched calibration, demonstrating the strong matrix tolerance of MICAP-MS, and its promising applicability to steel analysis.

Received 15th March 2023
Accepted 27th April 2023

DOI: 10.1039/d3ja00088e

rsc.li/jaas

Introduction

Iron can be processed by adding various alloying elements to produce steels with different elemental compositions and alloying grades, which are by far the most commonly used materials for man-made objects, from needles[1] to space rockets.[2] In addition to the alloying elements, specific mechanical or chemical properties of steels can be significantly influenced by trace elements, which are difficult or impossible to be removed during the steel smelting processes.[3] For example, it was reported that trace amounts of lead can promote the formation of abnormal graphites, which decreases crack resistance, tensile strength, and thermal shock.[4,5] Small amounts of aluminum can improve the toughness but significantly reduce the creep resistance, especially in the long term.[6,7] Furthermore, tin can be brought into the steel *via* the ferroalloys used for the melting process and can cause serious deterioration of the thermoplasticity, temper brittleness, and secondary hot working properties of steels.[8,9] Therefore, comprehensive characterization and quantification of the trace elements in steels are of great importance.

Inductively coupled plasma mass spectrometry (ICP-MS) has been successfully applied for trace element analysis due to its capability to measure trace levels of most elements of the periodic table.[10–12] In the last few decades, it has also been used for trace element analysis in steels.[13–15] However, a noticeable limitation in these measurements is the large contribution of metals to the matrix effects,[16,17] which may result in plasma suppression and long-term signal drift due to matrix deposition on the interface cones.[18,19] Due to the excessive influx of positively charged matrix ions space charge effects can occur, leading to the defocusing of the ion beam to the mass spectrometer.[20] Another limitation of the argon plasma sources is the interference resulting from Ar-related species. For example, $^{40}Ar^{+}$ and $^{40}Ar^{12}C^{+}$ can interfere with the most abundant isotopes of calcium and chromium, which restrict the characterization of these elements. Besides, the high consumption of Ar gas demands a substantial budget for its operation.

The Ar-related limitations have driven continued interest in the development of alternative sources for ICP.[21,22] Promising ion sources are microwave plasmas,[23,24] especially the recently developed nitrogen-based microwave inductively coupled atmospheric-pressure plasma (MICAP),[25–27] which utilizes a dielectric resonator in place of a load coil as in ICP, simplifying the instrument's electronics. By using nitrogen as

[a]*Bundesanstalt für Materialforschung und -prüfung (BAM), Richard-Willstätter-Str. 11, D-12489 Berlin, Germany. E-mail: Carlos.Abad@bam.de; Zengchao.You@bam.de*
[b]*Department of Chemistry, Humboldt Universität zu Berlin, Brook-Taylor-Str. 2, D-12489 Berlin, Germany*

† Electronic supplementary information (ESI) available. See DOI: https://doi.org/10.1039/d3ja00088e

a plasma gas, the typical Ar-related polyatomic interferents are not encountered. It has been demonstrated by several studies that MICAP-MS achieves comparable limits of detection (LOD) and sensitivity to ICP-MS for most of the elements, but costs significantly less for gas consumption.[26,28,29] For practical applications, the investigation of matrix effects in MICAP is of great interest. In the 1980s, Urh *et al.* developed a microwave-induced plasma optical emission spectrometer (MIP-OES), and showed that matrix effects in MIPs are much more severe than in the Ar-ICP.[30] About 30 years later, Thaler *et al.* implemented MICAP with OES in 2017, and demonstrated that matrix effects caused by sodium could suppress or enhance the analyte signal.[31] Thereafter, Pelipasov *et al.* further investigated the matrix effects induced by elements with different ionization potentials in MICAP-OES. They indicated that with a decrease in the ionization potential of the matrix elements, matrix effects for both atomic and ionic lines increase.[32] However, the influence of matrix effects in MICAP-MS has not been reported so far.

In the present work, we investigated the matrix tolerance of MICAP-MS and its applicability to quantification of minor components and trace elements in steels. The influences of gas flows and ion optics were studied. The recovery of the internal standards (IS) at different iron, nitric acid and hydrochloric acid concentrations was studied to evaluate the performance of MICAP-MS related to matrix tolerance without significantly compromising signal intensity. Non-alloy, low-alloy and high-alloy steels containing Al, V, Cr, Mn, Co, Cu, Ga, Nb, Mo, Pb, Sn, and Sb were analyzed after digestion with aqua regia, and the mass fractions of the selected elements were determined. Results obtained with aqueous and matrix-matched calibrations were compared and discussed.

Experimental

Materials and samples

The samples analyzed consisted of three steel certified reference materials EURONORM-CRM 096-2 (non-alloy steel, Bureau of Analyzed Samples Limited, United Kingdom), EURONORM-CRM 179-2 (alloyed steel, BAM, Germany), and EURONORM-CRM 286-1 (high-alloy steel, BAM, Germany). The three selected steel CRMs represent non-alloy, low-alloy and high-alloy steels. Following the classification from CEN/TR 10317 : 2020, a non-alloy steel has limit values for Si (max. 1%), Mn (max. 1.5%), Cr and Ni (max. 0.5% each), and Co, Cu, and W (max. 0.3% each) and no limit for C, P, B, S, or Pb. In low-alloy steels, at least one element has a higher content than the limits for non-alloy steels, but none exceeds 5%. The sum of all alloying elements is below 10%. In the case of high-alloy steels, at least one element has a higher content than 5%, or the sum of all alloying elements is above 10%. The Fe content is above 50%.

High-purity deionized water with a resistivity of 18 MΩ cm obtained from a Milli-Q system (Merck Millipore, Germany) was used throughout the experiments. HNO_3 (Merck AG, Germany), HCl (Merck AG, Germany), and HF (Merck AG, Germany) were used after purification by sub-boiling distillation in PFA containers. Calibration solutions were prepared from single-element standard solutions (Certipur®, Merck AG, Germany), and an ICP-MS IS solution (Analytik Jena GmbH, Germany) containing ^{6}Li, ^{45}Sc, ^{89}Y, ^{115}In, ^{159}Tb, and ^{209}Bi by dilution in 2% HNO_3. In addition, matrix-matched calibration solutions were spiked with an Fe plasma standard solution (Specpure®, Alfa Aesar, United Kingdom).

For parameters optimization, blank and matrix solutions each containing 50 μg L^{-1} IS in 2% HNO_3 were prepared. In addition, the matrix solutions contained 350 mg L^{-1} Fe, 90 mg L^{-1} Cr, and 40 mg L^{-1} Ni. All torch parameters (gas flow rates and sample depth) and ion optics parameters (voltages on lenses and mirrors) were tuned for high matrix tolerance and high sensitivity. For trace elements quantification, aqueous and matrix-matched calibrations were performed with six calibration levels. The calibration range and corresponding IS for each element can be found in Table S1.† Each calibration standard contained 50 μg L^{-1} IS in 2% HNO_3. In addition, 500 mg L^{-1} Fe was added to each standard for matrix-matched calibration, whereby no further elements were added for aqueous calibration.

Steel sample preparation

For ECRM 096-2 and ECRM 179-2, 50 mg of each were weighed, and then mixed with 5 ml water and 10 ml aqua regia. The mixtures were heated at 150 °C for 40 min. Then 0.5 ml HF was added, and the solution was left to stand at room temperature for 60 min. Finally, the solution was made up to 50 ml with water. For ECRM 286-1, 0.5 g of sample was weighed and mixed with 15 ml of aqua regia. The mixture was heated at 150 °C for 40 min, and then left to stand at room temperature for 60 min. Water was added to a final volume of 100 ml. All digestions were performed in triplicate. Before MICAP-MS measurement, digestion solutions were diluted 1 : 10, 1 : 100 and 1 : 500 in 2% HNO_3 with an IS concentration of 50 μg L^{-1}.

Instruments

A PlasmaQuant MS Elite quadrupole mass spectrometer (Analytik Jena GmbH, Germany) modified with a MICAP plasma source (Radom Research & Development, USA) was used for all experiments. Nitrogen (N_2 purity ≥ 99.999%, Linde AG, Germany) was used as a general nebulizer, auxiliary, and plasma gas. A peristaltic pump was used to transport the liquid samples to a concentric nebulizer (MicroMist, USA) combined with a cooled double-pass spray chamber. The liquid uptake rate of the peristaltic pump was approximately 500 μL min^{-1}. Aspect MS software (Analytik Jena GmbH, Germany) was used for data acquisition, including mass calibration, data processing, and plots. A linear calibration with internal standard correction was applied for each quantified element. The LOD was determined from the standard error of calibration, by dividing it by the slope and multiplying by 4. The limit of quantification (LOQ) is three times the LOD. The optimized operating conditions are listed in Table 1. Ion optics parameters can be found in Table S2.†

We found potential memory effects in the tubing for certain elements (V, Co, Nb, W). After two washing steps with 10%

Table 1 Optimized operation parameters used in MICAP-MS

MICAP-MS	
Plasma power	1500 W
Nebulizer gas flow	0.9 L min^{-1} N_2
Auxiliary gas flow	0.8 L min^{-1} N_2
Plasma gas flow	11 L min^{-1} N_2
Sampling depth	5 mm
Sampling cone	Pt 1.1 mm
Skimmer cone	Ni 0.5 mm

HNO_3, the signal returns to the blank level. Washing steps were performed after measurement of calibration standards and samples with high content of these elements.

Results and discussion

Influence of the operating conditions on the matrix tolerance

Matrix tolerance can be used to describe the robustness of an instrument to matrix effects, which is described by the signal intensity obtained from the matrix-loaded solution divided by the signal intensity obtained from matrix-free solution. To investigate the performance of MICAP-MS under matrix effects, matrix tolerance under different operating conditions was studied. To monitor the mass-based differentiation, six isotopes (^{6}Li, ^{45}Sc, ^{89}Y, ^{115}In, ^{159}Tb, and ^{209}Bi) with similar first ionization energy (IE) were used as IS. These elements cover a broad mass range, from 6 to 209, and are not found in the high-alloy steel matrix used for matrix tolerance optimization. They serve

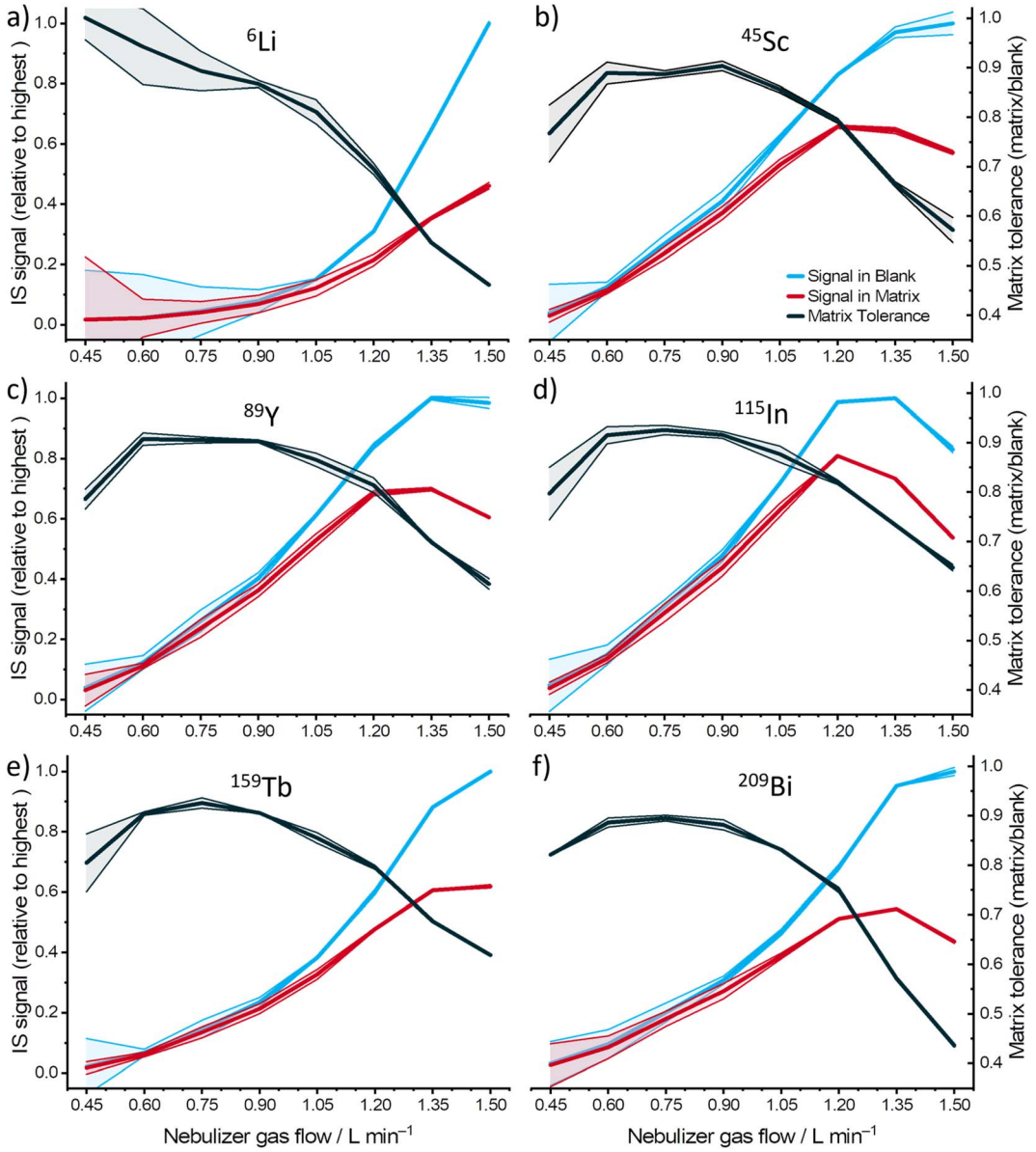

Fig. 1 Relative signal intensities of (a) ^{6}Li, (b) ^{45}Sc, (c) ^{89}Y, (d) ^{115}In, (e) ^{159}Tb and (f) ^{209}Bi in blank and matrix solutions (relative to the highest signal in the blank), and the corresponding matrix tolerance obtained using different nebulizer gas flow rates. The lines with light color represent the standard deviation of the measurement.

as representative indicators for all the elements being analyzed. An internal standard recovery between 80% and 120% is considered acceptable.

Since the degree of the matrix effect is strongly dependent on the applied nebulizer gas flow in ICP-MS, influences of the nebulizer gas flow on the matrix tolerance in MICAP-MS were studied first. IS intensities were monitored under varying nebulizer gas flow rates from 0.45 L min^{-1} to 1.5 L min^{-1}. Measurements were performed twice with blank and matrix solutions to give an insight into the variation of the matrix tolerance. The obtained results are shown in Fig. 1.

It can be observed that the signal intensities of the isotopes increased with a higher nebulizer gas flow rate, which was most likely due to the more efficient aerosol transport and ion sampling. However, a reduction could be observed for most of the isotopes (^{89}Y, ^{115}In, and ^{209}Bi) when the gas flow rate exceeded 1.35 L min^{-1}. This reduction might indicate that an excess aerosol load reduces the plasma temperature, ultimately leading to signal suppression.[33] Furthermore, this observation agrees with the MICAP-MS study reported by Kuonen *et al.*,[34] which indicates that higher nebulizer gas flow can also induce oxide formation in the plasma. ^{6}Li did not demonstrate this intensity reduction (see Fig. 1a), but it showed much lower intensity compared to other isotopes at a low gas flow rate, which might have resulted from the stronger ion diffusion in the plasma. Signal suppression could be observed in the results obtained with the alloy matrix. A clear reduction of the matrix tolerance occurred when a nebulizer gas flow rate higher than 0.9 L min^{-1} was applied. This reduction indicates that the matrix effect tends to be more severe at a high nebulizer gas flow rate, which might have resulted from the increased matrix plasma load and the shorter residence time of the aerosol. This reduction was especially obvious for ^{6}Li and ^{209}Bi (Fig. 1a and f), which was possibly caused by the increased space charge effect for the lighter ions, and the slightly higher first IE of Bi (7.3 eV), respectively. It has also been demonstrated that the non-linear mass dependency on the matrix effect was minimized by optimizing matrix tolerance. At a nebulizer flow rate of 0.9 L min^{-1}, the IS recovery in the matrix ranges from 87% to 92%. However, at a nebulizer flow rate of 1.35 L min^{-1} (optimized for high signal), not only does the recovery decrease, but the recovery range also becomes wider, spanning from 55% to 73%.

Apart from the nebulizer gas flow, influences of plasma gas flow, auxiliary gas flow, sheath gas flow, and sample depth on the matrix tolerance of MICAP-MS were also investigated. Fig. 2 shows the effects of varying conditions on ^{115}In. It can be observed in Fig. 2a and S1† that the plasma gas flow did not significantly influence the plasma intensity and matrix

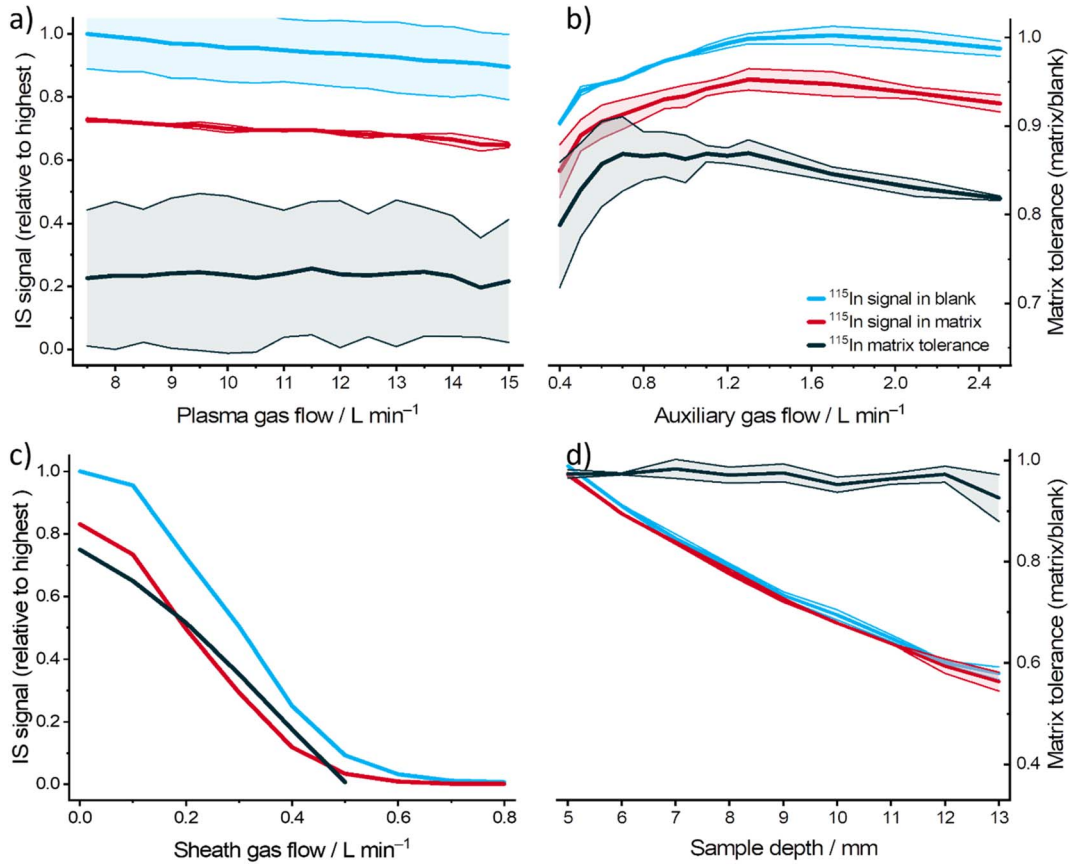

Fig. 2 Relative signal intensities of ^{115}In in blank and matrix solutions (relative to the highest signal in the blank), and the corresponding matrix tolerance obtained using different (a) plasma gas flows, (b) auxiliary gas flows, (c) sheath gas flows, and (d) sample depths. The lines with light color represent the standard deviation of the measurement.

tolerance, since it is the outer gas flow in the plasma torch. The auxiliary (intermediate) gas flow showed a similar tendency to the nebulizer gas flow, especially for ^{6}Li and ^{209}Bi (see Fig. S2†). However, its influence is less pronounced. Sheath gas flow is the nitrogen gas flow after nebulization, which surrounds the aerosol. Increasing the sheath gas flow rate and sampling depth could reduce the signal intensity (see Fig. 2c and d, S3 and S4†), possibly due to the reduced aerosol transport efficiency. Moreover, no improvement in the matrix tolerance could be observed after increasing these two parameters.

To investigate the influence of ion optics in MICAP-MS, the voltages applied to various ion optics were optimized and compared (see Fig. S5–14†). As examples, the results obtained with ^{6}Li and ^{115}In using different first lens and right mirror voltages are shown in Fig. 3. For ^{115}In, the lens and mirror voltages had no significant influence on the matrix tolerance, whereas a noticeable improvement or deterioration effect could be observed for ^{6}Li. A possible explanation is that due to the lighter ion mass, Li was more significantly affected by the inelastic collision with the N_2 residual gas molecules behind the skimmer cone, reducing the number of ions transported to the mass analyzer. Therefore, optimizing ion optics could improve the ion transport efficiency and correspondingly reduce the influence of this matrix effect on light elements. Similar to ICP-MS, mass bias could also be observed in the ion optics of MICAP-MS, where the ions with elevated masses demonstrated shifted optimum voltages (see Fig. S15 and S16†).

When optimizing the parameters for plasma conditions and ion optics, the selection criterion was the average matrix tolerance for all six elements under investigation. In cases where matrix tolerance was not significantly affected, the criterion shifted to the average signal intensity. This approach represents a compromise. But the optimization of the average coincides, to a certain extent, with the optimization of element ^{115}In, which is situated at the midpoint of the mass range.

Matrix tolerance of MICAP-MS at different Fe matrix concentrations

After parameters optimization, the matrix tolerance of the MICAP-MS was investigated by measuring the intensity recoveries of ^{45}Sc, ^{89}Y, ^{115}In, ^{159}Tb, and ^{209}Bi in 2% HNO_3 with Fe concentrations ranging from 10 mg L^{-1} to 5000 mg L^{-1}. The optimized parameters used for these measurements are listed in Tables 1 and S2.†

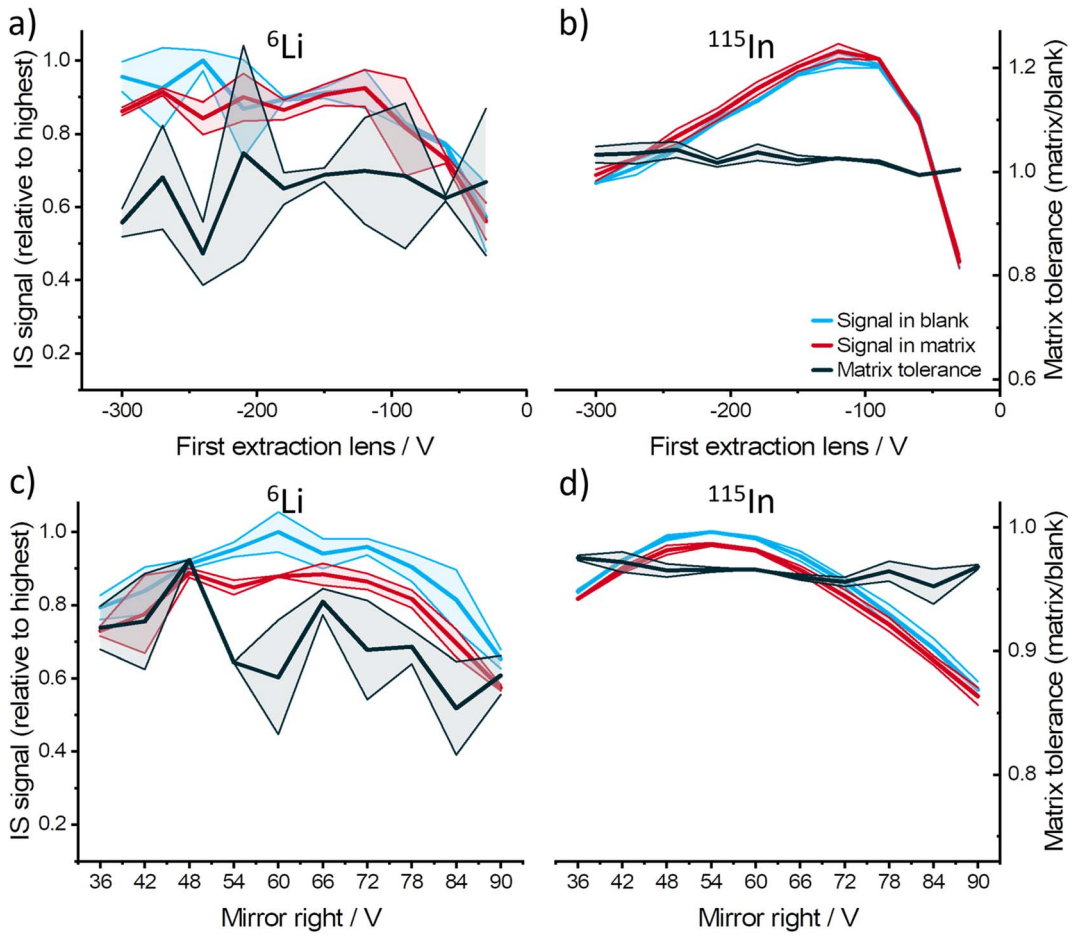

Fig. 3 Relative signal intensities of ^{6}Li and ^{115}In in blank and matrix solutions (relative to the highest signal in the blank), and the corresponding matrix tolerance obtained using different (a and b) first lens voltages and (c and d) right mirror voltages. The lines with light color represent the standard deviation of the measurement.

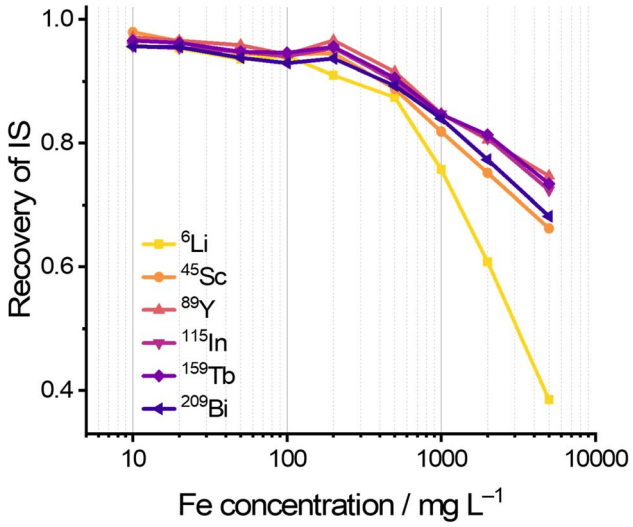

Fig. 4 Intensity recovery of ^{45}Sc, ^{89}Y, ^{115}In, ^{159}Tb, and ^{209}Bi in 2% HNO_3 with different Fe concentrations in relation to the IS solution with no matrix.

Fig. 4 shows that despite the Fe-induced matrix effects, the recovery rates of all elements remained above 90% at an Fe concentration of 500 mg L^{-1}. Even at an Fe concentration of 1 g L^{-1}, the recovery rates remained above 80%, which demonstrates the strong matrix tolerance of MICAP-MS. Influences of the acid content on the matrix tolerance were also investigated by performing the measurements with HNO_3 and HCl, whose concentrations range from 2% to 25%. It can be observed in Fig. S17† that high acid concentration leads to signal suppression for most of the elements in MICAP-MS. Both signal suppression and enhancement were observed for ^{6}Li. This agrees with the theory described by Stewart and Olesik[35,36] for Ar-based ICP-MS, which revealed that increasing the acid concentration could alter the aerosol evaporation, volumetric flux, and size distribution in the spray chamber. Consequently, the transport efficiency and the signal intensity could be reduced.

It is noteworthy that we observed significant matrix deposition on the sample cone during our experiments. However, after an initial period of deposition, the signal stabilized, which can be attributed to the minimal matrix effect. A method focusing on higher signal intensity might reveal a more drifting signal as matrix deposition on the sample cone progresses. Upon cleaning the sample cone and allowing initial deposition to occur again, the signal reached a stable state again. Throughout the entire calibration and sample measurement campaign, no further cleaning was required.

Characterization of the reference steel samples

To validate the observed matrix tolerance of MICAP-MS in the Fe matrix, non-alloy steel ECRM 096-2, alloyed steel ECRM 179-2, and high-alloy steel ECRM 286-1 were digested and analyzed. Aqueous and matrix-matched calibrations were performed to investigate the influence of matrix effects. Isotopes used for quantification are shown in Table S3.† The choice of isotopes for analysis was based on their abundance, the absence of non-isobaric overlap from other elements, and polyatomic ion interferents from the plasma. Each steel sample was digested in triplicate. The mass fractions obtained are the average values of the threefold measurements and are shown in Table 2. The ζ-score indicates the metrological compatibility between the experimental data and the reference values. The calculation is

Table 2 Comparison of trace elements and minor components mass fractions in ECRM 096-2, ECRM 179-2, and ECRM 286-1 determined by MICAP-MS using aqueous and matrix-matched calibration with the reference values

		Reference		Aqueous calibration			Matrix-matched calibration		
Elements		Mean	SM	Mean	SD	ζ-Score	Mean	SD	ζ-Score
096-2	Mn (%)	1.320	0.012	1.330	0.016	0.5	1.335	0.016	0.8
	Cr (%)	0.0243	0.0009	0.0253	0.0001	1.1	0.0251	0.0001	0.9
	Mo (%)	0.0020	0.0003	0.0020	0.0000	0.0	0.0019	0.0000	−0.3
	Al (%)	0.0460	0.0011	0.0456	0.0003	−0.4	0.0469	0.0004	0.8
	Cu (%)	0.0170	0.0005	0.0160	0.0005	−1.4	0.0177	0.0004	1.1
	Nb (%)	0.025	0.001	0.0252	0.0008	0.0	0.0240	0.0007	−1.0
179-2	Mn (%)	0.539	0.009	0.543	0.011	0.3	0.555	0.011	1.1
	Cr (%)	1.08	0.03	1.090	0.022	0.1	1.085	0.022	0.0
	Mo (%)	0.070	0.006	0.0716	0.0009	0.3	0.0704	0.0009	0.1
	Cu (%)	0.111	0.004	0.116	0.003	1.1	0.116	0.003	1.1
	V (%)	0.188	0.007	0.206	0.005	2.1	0.200	0.005	1.4
	Ga (%)	0.00129	0.00017	0.00128	0.00003	0.0	0.00100	0.00002	−1.8
	Nb (%)	0.00144	0.00018	0.00151	0.00002	0.4	0.00148	0.00002	0.2
	Sb (%)	0.00175	0.00017	0.0020	0.0003	0.6	0.0025	0.0003	1.9
286-1	Mn (%)	1.919	0.025	1.970	0.008	1.9	1.971	0.008	2.0
	Mo (%)	0.329	0.009	0.338	0.005	0.9	0.337	0.004	0.9
	Co (%)	0.151	0.008	0.159	0.001	1.1	0.152	0.001	0.2
	Sb (%)	0.0014	0.0004	0.0020	0.0002	1.3	0.0019	0.0002	1.1
	Sn (%)	0.0084	0.0009	0.0092	0.0001	0.9	0.0093	0.0001	1.0
	Pb (%)	0.00028	0.00013	0.00024	0.00001	0.3	0.00024	0.00001	0.3

performed according to DIN ISO 13528:2020-09 and is shown in eqn (1). In the equation, χ_i denotes the measured value, and $u(\chi_i)$ refers to its associated standard deviation (SD). Similarly, χ_{pt} represents the interlaboratory mean, while $u(\chi_{pt})$ is the standard deviation of that mean (SM). The results are metrologically compatible, when the absolute of the ζ-score is less than or equal to 2.

$$\zeta_i = \frac{x_i - x_{pt}}{\sqrt{u^2(x_i) + u^2(x_{pt})}} \quad (1)$$

The results obtained with aqueous and matrix-matched calibration for most elements were comparable and agreed well with the reference values. This indicates that no significant signal suppression or enhancement was observed during the measurements. However, the determined mass fraction of ^{51}V in ECRM 179-2 was slightly higher than the reference value, which might have resulted from the polyatomic ion interferent $^{14}N^{37}Cl$. Moreover, the LOD and LOQ determined with different calibration methods were in the same order of magnitude for most elements (see Table S3†). As the skimmer cone used is made of Ni, it was not quantified in the steel samples. Cr and W serve as the primary alloying elements in ECRM 286-1 and ECRM 179-2, respectively. The high contents of these elements are not in the working range of the method.

Conclusions

This work demonstrates the suitability of MICAP-MS as a reliable technique with promising matrix tolerance for trace element analysis in steels. Influences of operating conditions on matrix tolerance were investigated by systematically varying the gas flow rates and ion optics voltages while monitoring the intensity variation of ^{6}Li, ^{45}Sc, ^{89}Y, ^{115}In, ^{159}Tb, and ^{209}Bi in blank and matrix solutions. It was concluded that the nebulizer gas flow had the most significant influence on the matrix tolerance. With increasing nebulizer gas flow rate, the matrix tolerance decreased due to stronger matrix plasma load and shorter residence time of the aerosol in the plasma. Besides, ^{6}Li suffered more from the matrix effects at high nebulizer gas flow, which might have resulted from the stronger space charge effect before the sample cone due to its light mass. ^{209}Bi also showed lower matrix tolerance at a high nebulizer gas flow rate, possibly related to its slightly higher first IE. Other gas flows, including plasma, auxiliary, and sheath gas did not show obvious influence on the matrix tolerance. Only the auxiliary gas flow could slightly alter the matrix tolerance, whereas the magnitude is weaker than that of the nebulizer gas flow. Ion optics showed promising effects on improving the matrix tolerance of ^{6}Li, mainly due to the reduction of the inelastic collisional scattering effect behind the skimmer cone. No significant effect was observed for heavier elements since the collision with the N_2 residual gas molecules affects them less.

With optimized operating conditions, MICAP-MS showed high matrix tolerance, which achieved an intensity recovery of more than 90% at an Fe concentration of 500 mg L^{-1} and 80% at 1000 mg L^{-1}. Like Ar-based ICP-MS,[35,36] high acid concentration could result in intensity suppression in MICAP-MS, which might relate to changes in aerosol transport efficiency. The mass fractions of Al, Mn, Mo, Co, Cr, Mo, Cu, V, Ga, Nb, Sb, Sn, and Pb in the reference steel samples determined by MICAP-MS were comparable and compatible with the reference values. No significant difference was observed between the results obtained with aqueous and matrix-matched calibration. The LOD and LOQ determined with different calibration methods were also mostly in the same magnitude, which validates the excellent matrix tolerance of MICAP-MS. This study proves the applicability of MICAP-MS to element analysis in steels, with reduced matrix effect of Fe including primary alloying elements (Ni, Cr, Mn, W) with similar first ionization energy and atomic radii. The quantification covers a wide concentration range over five orders of magnitude from trace elements to minor components. Future research could expand on this work by exploring the matrix effect of easily ionizable elements such as Ca, Na, K, and Li in MICAP-MS, potentially broadening its applicability even further.

Conflicts of interest

There are no conflicts to declare.

Acknowledgements

The authors are grateful for the support from Analytik Jena GmbH. This work was supported by the Bundesanstalt für Materialforschung und -prüfung (BAM) with the funding program “Menschen – Ideen” project number IE2120.

References

1 C. H. Barbosa, E. C. Monteiro, E. A. Lima, S. F. Santos, E. G. Cavalcanti and P. C. Ribeiro, *IEEE Trans. Appl. Supercond.*, 2001, **11**, 677–680.
2 S. V. S. N. Murty, G. S. Rao, A. Venugopal, P. R. Narayanan, S. C. Sharma and K. M. George, *Metall. Microstruct. Anal.*, 2014, **3**, 433–447.
3 A. Ramadan, A. Y. Shash, I. S. El-Mahallawi, D. Senk and T. Mattard, *J. Iron Steel Res. Int.*, 2015, **22**, 582–589.
4 H. M. Muhmond and H. Fredriksson, *Metall. Mater. Trans. A: Phys. Metall. Mater. Sci.*, 2014, **45**, 6187–6199.
5 K. Ankamma, *J. Inst. Eng. India Ser. D*, 2014, **95**, 19–26.
6 H. Naoi, M. Ohgami, X. Liu and T. Fujita, *Metall. Mater. Trans. A: Phys. Metall. Mater. Sci.*, 1997, **28**, 1195–1203.
7 M. F. Eldridge and R. C. Cochrane, in *Proceedings of the International Conference on Microalloying in Steels*, ed. J. M. RodriguezIbabe, I. Gutierrez and B. Lopez, 1998, vol. 284–2, pp. 217–224.
8 X. Zhang, G. J. Ma, M. K. Liu and Z. Li, *Metals*, 2019, **9**(8), 834.
9 C. Nagasaki and J. Kihara, *ISIJ Int.*, 1997, **37**, 523–530.
10 R. Dolan, J. Vanloon, D. Templeton and A. Paudyn, *Fresenius. J. Anal. Chem.*, 1990, **336**, 99–105.
11 N. Laur, R. Kinscherf, K. Pomytkin, L. Kaiser, O. Knes and H. P. Deigner, *PLoS One*, 2020, **15**, e0233357.

12 M. J. Duane and S. Facchetti, *Sci. Total Environ.*, 1995, **172**, 133–144.
13 E. S. Steenstra, J. Berndt, S. Klemme and W. van Westrenen, *J. Anal. At. Spectrom.*, 2019, **34**, 222–231.
14 T. Luo, Y. Wang, M. Li, W. Zhang, H. H. Chen and Z. C. Hu, *At. Spectrosc.*, 2020, **41**, 11–19.
15 J. Y. Hu and H. Z. Wang, *Mikrochim. Acta*, 2001, **137**, 149–155.
16 S. H. Tan and G. Horlick, *J. Anal. At. Spectrom.*, 1987, **2**, 745–763.
17 P. Holdship, P. Bonnand, D. Price and P. Watson, *J. Anal. At. Spectrom.*, 2018, **33**, 1941–1953.
18 R. C. Hutton and A. N. Eaton, *J. Anal. At. Spectrom.*, 1988, **3**, 547–550.
19 Q. Zhang, J. T. Snow, P. Holdship, D. Price, P. Watson and R. E. M. Rickaby, *J. Anal. At. Spectrom.*, 2018, **33**, 1196–1208.
20 N. Praphairaksit and R. S. Houk, *Anal. Chem.*, 2000, **72**, 2356–2361.
21 S. F. Durrant, *Fresenius. J. Anal. Chem.*, 1993, **347**, 389–392.
22 C. I. M. Beenakker, *Spectrochim. Acta, Part B*, 1976, **31**, 483–486.
23 Y. Okamoto, M. Yasuda and S. Murayama, *Jpn. J. Appl. Phys., Part 2*, 1990, **29**, L670–L672.
24 K. Oishi, T. Okumoto, T. Iino, M. Koga, T. Shirasaki and N. Furuta, *Spectrochim. Acta, Part B*, 1994, **49**, 901–914.
25 A. Müller, D. Pozebon and V. L. Dressler, *J. Anal. At. Spectrom.*, 2020, **35**, 2113–2131.
26 C. Neff, P. Becker, B. Hattendorf and D. Gunther, *J. Anal. At. Spectrom.*, 2021, **36**, 1750–1757.
27 A. J. Schwartz, Y. Cheung, J. Jevtic, V. Pikelja, A. Menon, S. J. Ray and G. M. Hieftje, *J. Anal. At. Spectrom.*, 2016, **31**, 440–449.
28 M. Schild, A. Gundlach-Graham, A. Menon, J. Jevtic, V. Pikelja, M. Tanner, B. Hattendorf and D. Gunther, *Anal. Chem.*, 2018, **90**, 13443–13450.
29 Z. C. You, A. Akkus, W. Weisheit, T. Giray, S. Penk, S. Buttler, S. Recknagel and C. Abad, *J. Anal. At. Spectrom.*, 2022, **37**, 2556–2562.
30 J. J. Urh and J. W. Carnahan, *Appl. Spectrosc.*, 1986, **40**, 877–883.
31 K. M. Thaler, A. J. Schwartz, C. Haisch, R. Niessner and G. M. Hieftje, *Talanta*, 2018, **180**, 25–31.
32 O. V. Pelipasov and E. V. Polyakova, *J. Anal. At. Spectrom.*, 2020, **35**, 1389–1394.
33 C. Agatemor and D. Beauchemin, *Anal. Chim. Acta*, 2011, **706**, 66–83.
34 M. Kuonen, G. Niu, B. Hattendorf and D. Günther, *J. Anal. At. Spectrom.*, 2023, **38**, 758–765.
35 I. I. Stewart and J. W. Olesik, *J. Anal. At. Spectrom.*, 1998, **13**, 1313–1320.
36 I. I. Stewart and J. W. Olesik, *J. Anal. At. Spectrom.*, 1998, **13**, 843–854.